

1 **Fe-periclase reactivity at Earth's lower mantle conditions: *ab-initio***
2 **geochemical modelling**

3
4 Marcello Merli¹, Costanza Bonadiman², Valeria Diella³, Luciana Sciascia²,
5 Alessandro Pavese⁴

6
7 ¹ *Department of Earth and Marine Sciences, University of Palermo, Via Archirafi 36, 90123*
8 *Palermo, Italy.*

9 ² *Department of Physics and Earth Sciences, University of Ferrara, Via Saragat 1, 44122 Ferrara,*
10 *Italy*

11 ³ *Consiglio Nazionale delle Ricerche, CNR-IDPA, Sezione di Milano, Via Botticelli 23, 20133*
12 *Milano, Italy*

13 ⁴ *Department of Earth Sciences "A. Desio", University of Milan, Via Botticelli 23, 20133 Milan,*
14 *Italy*

15
16 Correspondence: Alessandro Pavese

17 e-mail: alessandro.pavese@unimi.it

18
19 **key-words:** MgO-FeO binary; pyrolitic geochemical model; lower mantle geochemical
20 heterogeneities; subsolidus reaction modelling; mixing Gibbs energy

21 **ABSTRACT**

22 Intrinsic and extrinsic stability of the (Mg,Fe)O solid mixture in the Fe-Mg-Si-O system at high P,T
23 conditions relevant to the Earth's mantle is investigated by the combination of quantum mechanical
24 calculations (Hartree- 26 Fock/DFT hybrid scheme), cluster expansion techniques and statistical
25 thermodynamics. Iron in the (Mg,Fe)O binary mixture is assumed to be either in the low spin (LS)
26 or in the high spin (HS) state. Un-mixing at solid state is observed only for the LS condition in the
27 23-42 GPa pressure range, whereas HS does not give rise to un-mixing. LS (Mg,Fe)O un-mixings
28 are shown to be able to incorporate iron by subsolidus reactions with a *reservoir* of a virtual
29 bridgmanite composition, for a maximum *total* enrichment of ~ 0.22 FeO. At very high P (up to
30 130/3150 GPa/K), a predominant (~ 0.7 phase proportion), iron-rich Fe-periclase mixture
31 $(\text{Mg}_{0.50}\text{Fe}_{0.50})\text{O}$ is formed, and it coexists, at constrained phase composition conditions, with two
32 iron-poor assemblages $[(\text{Mg}_{0.90}\text{Fe}_{0.10})\text{O}$ and $(\text{Mg}_{0.825}\text{Fe}_{0.175})\text{O}]$. These theoretical results agree with
33 the compositional variability and frequency of occurrence observed in lower mantle Fe-periclase
34 from diamond inclusions and from $HP-HT$ synthesis products. The density difference among the
35 Fe-periclase phases increases up to $\sim 10\%$, between 24 and 130 GPa. The calculated bulk Fe/Mg
36 partitioning coefficient between the bridgmanite *reservoir* and Fe-periclase, K_d , is 0.64 at 24 GPa;
37 it then drops to 0.19 at 80 GPa, and becomes quasi-invariant (0.18-0.16) in the lowermost portion of
38 the Earth's mantle (~ 80 -130 GPa). These K_d -values represent an approximate estimate for the
39 Fe/Mg-partitioning between actual bridgmanite and Fe-periclase. Consequently, our K_d -values
40 agree with experimental measurements and theoretical determinations, hinting that iron
41 preferentially dissolves in periclase with respect to all the other iron-bearing phases of the lower
42 mantle. The continuous change up to 80 GPa (~ 2000 km depth) of the products (compositions and
43 phase proportions) over the MgO-FeO binary causes geochemical heterogeneities throughout the
44 lower mantle, but it does not give rise to any sharp discontinuity. In this view, anomalies like the
45 ULVZs, explained with a local and abrupt change of density, do not seem primarily ascribable to
46 the mixing behavior and reactivity of (Mg,Fe)O at subsolidus.

47 1. INTRODUCTION

48

49 1.1 (Mg,Fe)O-system

50

51 The Earth's lower mantle is home to some of the most fascinating problems related to the interior of
52 our planet, ranging from sharp discontinuity to anisotropy and unresolved geochemical processes,
53 *i.e.* origins of mantle plumes, segregation of dense sub-ducted slab components, residual of core
54 formation processes and core/mantle chemical exchange (Albarede and vander Hilst, 2002).

55 All the Earth Reference models (*e.g.* PREM and AK135; Dziewonski and Anderson, 1981; Kennett
56 et al., 1995), which are designed to match whole Earth mechanical properties and astrophysical
57 data, agree to indicate Fe-periclase and (Mg,Fe)-perovskite (bridgmanite) as the main phases of the
58 lower mantle bulk phase-composition. Therefore, the reactions involving the subsolidus MgO-FeO
59 system (*i.e.* Fe-periclase phase) provide a relevant contribution to the general geochemical
60 behaviour of the lower mantle. Seismic anomalies are associated to geochemical discontinuities,
61 such as those of the D''-layer (Lay and Helmberger, 1983; Sidorin et al., 1999; Kaneshima and
62 Helffrich, 1999; Murakami et al. 2012) and ULVZs (McNamara et al., 2010), in the lowermost
63 portion of the Earth's mantle. Geochemical perturbations in this region are ascribed to diverse
64 possible causes, some of which are related to the Fe content and its distribution in the lower mantle
65 phases, *i.e.*: (i) high-to-low spin state transition of iron in Fe-periclase (Dobson and Brodholt, 2005;
66 Mao et al., 2006; Lin et al., 2013; Zhang et al., 2016); (ii) appearance of new phases, *e.g.* a post-
67 perovskite, Fe-segregation in iron-bearing phases, Si-Mg-Fe melts and partially molten systems
68 (Trampet et al., 2004; Murakami et al. 2005, 2012; da Silva et al., 2000; Karki et al., 2001;
69 Wentzcovitch et al., 2004; Garner, 2004; Lay et al., 2004; Nomura et al., 2011; Andrault et al.,
70 2011; Thorne et al., 2013, Zhang et al., 2016).

71 Although the (Mg,Fe)O solid mixture at high pressure and high temperature conditions (HP-HT)
72 has been largely investigated (*e.g.*: Vassiliou and Ahrens, 1982; Fei et al., 1992; Richet et al., 1989;

73 Dubrovinsky et al. 2000; 2001; Kung et al., 2002; Jacobsen et al., 2004; 2006; Zhang and Kostak,
74 2002; van Westrenen et al., 2005; Jackson et al., 2006; Lin et al, 2009), several questions are still
75 open, *i.e.* the un-mixing process and the highest allowed Fe content in the lower mantle Fe-
76 periclase. Some authors (*e.g.*: Lin et al., 2003; Ohta et al., 2014) do not observe un-mixing of
77 (Mg,Fe)O in static compression experiments, whereas others (Dubrovinsky et al. 2000; 2001)
78 report a gradual formation of magnesium-rich and iron-rich oxide phases from (Mg,Fe)O at P and
79 T above 80 GPa and about 1000 K, respectively. In addition, Fe-periclase obtained by HP-HT
80 Fe/Mg partitioning experiments from a starting material bearing 0.1-0.3 FeO (Auzende et al., 2008;
81 Sinmyo et al., 2008, Nakajima et al., 2012; Prescher et al., 2014) shows a wide compositional range
82 (0.088-0.487 FeO) with respect to the coexisting (Mg,Fe)-perovskite (0.026-0.161 FeO). These
83 results are in keeping with observations of lower mantle Fe-periclase findings (~0.15-0.70 FeO) that
84 occur as inclusions in diamonds (Kaminsky, 2012 and reference therein). It is worth noting that
85 ~0.3-0.5 FeO natural compositions (Kaminski, 2012) have a relevant statistical occurrence (55 out
86 of 230 samples), whereas Mg-wüstite (0.5-0.7 FeO) is rarely observed (6 out of 230 samples). Such
87 a variety, in terms of Fe-periclase compositions, is difficult to be explained in the frame of the
88 extant experimental works on un-mixing processes (*i.e.* Ohta et al., 2014 and reference therein). All
89 this has led some authors (Javoy et al., 2010; Kaminsky, 2012) to ultimately invoke a different
90 reference Earth model (enstatite/chondrite *versus* pyrolite) to account for the bulk lower mantle
91 composition (Badro et al., 2003; Irifune et al. 2010; Mao et al. 2006; Matas et al, 2007).

92 In this work the miscibility of (Mg,Fe)O and possible disequilibrium reactions with a *reservoir*,
93 which complements the Fe-periclase in the formation of the bulk lower mantle, are investigated and
94 the results of our study are compared with observations.

95 The bulk lower mantle was split into two different geothermal regions: the lower mantle (LM) and
96 the lowermost lower mantle (LLM). LM accounts for the mantle region well below the transition
97 zone (>23 GPa; >700 Km) and above the perturbed D''-layer, and exhibits relatively smooth trends
98 of seismic profiles. In this view, LM can be considered as a seismically and chemically

99 homogeneous lower mantle portion, along a given model geotherm. LLM, in turn, refers to the
100 lowermost region of the Earth's mantle (>80 GPa; >2000 Km), where deviations in the seismic
101 profiles suggest changes of the P - T regime and phase composition, with respect to LM's. LM and
102 LLM are **assumed** to be undistinguishable in terms of bulk geochemical model.

103

104 **1.2 Deviations from ideality**

105

106 The present modelling aims to provide a global view of the Fe-periclase compositional trend that
107 stabilises along a chosen geotherm. In order to achieve this, some simplifications were inevitably
108 introduced.

109 First, the effects of plastic deformation were neglected. In the Fe-periclase/bridgmanite system, the
110 former is supposed to accommodate most of the plastic deformation, which develops through
111 dislocation creeps (Madi et al, 2005). However, much uncertainty still exists about the actual
112 mechanism driving such a phenomenon, its relation to composition and its occurrence throughout
113 the lower mantle (Reali et al, 2017; Girard et al, 2016; Cordier et al, 2012; Tommaseo et al, 2006).
114 Van Orman et al. (2003) observed that the occurrence of dislocations in Al-doped MgO does not
115 seem to extensively affect cation diffusion. This suggests that dislocations modestly influence the
116 octahedral-site force field in periclase, which still preserves its crystal structure and is affected by
117 plastic deformation processes (see the authors quoted above). An approximate estimate of the ratio
118 between energy due to "dislocations" (*i.e.* $\frac{1}{2} G_{\text{shear modulus}} \times b_{\text{Burgers vector}}^2 \times \rho_{\text{dislocation density}} \times V$) and
119 elastic energy of "hydrostatic deformation" (*i.e.* $P \times (V - V_0)$) gives a value of $\sim 10^{-3}$, using the
120 periclase's elastic constants and dislocation density from Zha et al (2000) and Miyajima et al
121 (2014), respectively. Given that the deformation energy is mostly due to its hydrostatic/elastic
122 contribution we think it reasonable to neglect the dislocation effects.

123 Another important simplification was to ignore ferric iron. First of all, lower mantle ferric iron is
124 experimentally predicted to preferentially enter bridgmanite (Frost and Myhill, 2016; Kurnosov et

125 al. (2017). In addition, Fe^{3+} is theoretically associated to the appearance of vacancies in non-
126 stoichiometric wüstite and $(\text{Mg,Fe})\text{O}$ (Wdowik et al. 2015; Otsuka et al. 2010). Measured iron in
127 Fe-periclase and bridgmanite, both coexisting as inclusions in lower-mantle diamonds (Kaminsky
128 and Lin (2017), reveals that Fe^{3+} un-mixes from periclase lattice, giving rise to clusters of
129 $(\text{Mg}_{1+x}\text{Fe}^{3+}_{2-x})\text{O}_{4-x/2}$. The iron related to Fe-periclase and un-mixed clusters is inferred to be
130 $\text{Fe}^{3+}/\Sigma\text{Fe}$ 8-12 at%. Given that most iron content values in natural $(\text{Mg,Fe})\text{O}$ do not exceed 0.5 FeO
131 (Harte, 2010; Kaminsky, 2012), the vacancy generation effect induced by ferric iron can therefore
132 be assumed negligible in the present modelling.
133 Finally, the potential effects of metallization of iron were neglected since such a reaction is
134 experimentally observed only in *quasi-wüstite* compositions (Otha et al. 2014).

135

136 2. LOWER MANTLE GEOCHEMICAL FRAME

137

138 The pyrolite model provides one of the possible chemical compositions for the Earth's lower
139 mantle. On the basis of phase equilibrium principles and known physical properties of HP minerals,
140 the lower mantle turns out to be mainly constituted of $(\text{Mg,Fe})\text{SiO}_3$ (bridgmanite), $(\text{Mg,Fe})\text{O}$ (Fe-
141 periclase) and CaSiO_3 (Ca-perovskite), besides an “undefined HP Al-phase” (i.e. Miyajima et al.,
142 2001; Pamato et al., 2014). Such phases occur in proportions that are a function of both
143 geochemical and geophysical models. The former constrains the bulk chemical composition
144 (McDonough and Sun, 1995; Lyubetskay and Korenaga, 2007; Stixrude and Lithgow-Bertelloni,
145 2007; Merli et al. 2016); the latter accounts for density-pressure-temperature profiles that are
146 consistent with observations (*i.e.*: seismic velocities, density and bulk sound speed; Jackson 1998,
147 Mattern et al. 2005; de Wit and Trampet, 2015).

148 Assuming the mantle to be representable by the CMASF system ($\text{CaO-MgO-Al}_2\text{O}_3\text{-SiO}_2\text{-FeO}$), the
149 pyrolitic model's phase composition of the lower mantle consists of ~75-78 wt% $(\text{Mg,Fe})\text{SiO}_3$, ~6-
150 10 wt% CaSiO_3 , ~15 wt% $(\text{Mg,Fe})\text{O}$ and ~2 wt% high-pressure Al-rich phase (Ono and

151 Oganov, 2005; Mainprice, 2007; Merli et al., 2016). Given that Ca-perovskite and bridgmanite
152 exhibit similar thermoelastic responses at the reference lower mantle P - T conditions (Deschamps
153 and Trampert, 2004; Matas et al, 2007; Li et al. 2005), a simplified MgO-SiO₂-FeO system (MSF)
154 was used in the present work.

155 The conversion from CMASF to MSF consists in replacing Mg+Ca+Al/2 with Mg, and Si+Al/2
156 with Si. The resulting bulk chemical composition (Table 1) has a Mg/Si molar ratio of 1.20, which
157 is lower than the pyrolitic value (~ 1.27) but higher than the chondritic one (~ 1.1). Such a ratio is in
158 agreement with a lower bulk chemical composition slightly enriched in SiO₂ (and FeO) and
159 depleted of MgO, with respect to the pristine pyrolitic model (Deschamps and Trampert, 2004;
160 Matas et al., 2007; Merli et al., 2016). The fractions by weight of Fe-periclase and bridgmanite in
161 the lower mantle were estimated 0.13 and 0.87 (Table 1) respectively, by means of least-square
162 mass balance calculations (Paktunc, 1998; Kobayashi et al., 2005) under the constraint of the LM-
163 LLM bulk chemical composition.

164 A geotherm (Fig.1) with a potential temperature of 1920 K at 24 GPa and T -vertical-gradient
165 (dT/dz) of ~ 0.5 K/Km (Matas et al., 2007; Ono, 2008; Merli et al., 2016) was assumed for LM
166 (~ 700 - 1900 Km depth). A geotherm (>80 GPa; >2000 Km) with a potential temperature of 2615 K
167 at 96 GPa and a higher T -gradient than LM's, *i.e.* $dT/dz \sim 0.85$ K/Km (Deschamps and Trampert,
168 2004; de Koker, 2010; Wicks et al., 2010; de Wit and Trampert, 2015), was instead chosen for LLM
169 (Fig.1).

170

171 3. THERMODYNAMIC APPROACH

172

173 The mixing of the MgO and FeO components in the periclase structure was modelled by extending
174 to the HP-regime the formalism of Merli et al (2015) that uses discrete Chebychev polynomial
175 expansions (Barnard et al. 1998) and statistical thermodynamics (Sanchez et al, 1984). A Hartree-

176 Fock/DFT hybrid scheme was adopted to carry out quantum energy calculations (Dovesi et al.
177 2009) on super-cells.

178 179 **3.1 Gibbs energy of mixing at high-pressure and high-temperature**

180
181 A given Fe-periclase composition, expressed by $x=\text{Fe}/(\text{Fe}+\text{Mg})$ and $(1-x)=\text{Mg}/(\text{Fe}+\text{Mg})$, is
182 compatible with many Mg-Fe configurations (Λ), each one corresponding to a specific arrangement
183 of the magnesium and iron atoms. In the frame of the isothermal-isobaric ensemble a system is
184 composed of N particles at equilibrium with P and T (*i.e.* NPT -ensemble). For simplicity, we do not
185 take into account the explicit dependence on P and T of the thermodynamic potentials, except for
186 the functions $\Xi(P,T,x)$ and $\xi(P,T,x)$, which are related to the NPT -ensemble.

187 $\Xi(P,T,x)$ is defined by Dill et al. (2003) as:

$$188 \quad \Xi(P,T,x) = \sum_{\Lambda=1,n} \exp[-H(x,\Lambda)/kT] = \sum_{\Lambda=1,n} \exp[-(U(x,\Lambda)_{st} + PV(x,\Lambda)_{st})/kT] \times Z(x,\Lambda)_{vib} \quad (1)$$

189 where n is the number of all the possible configurations.

190 The Gibbs function is related to $\Xi(P,T,x)$ in terms of

$$191 \quad G(x) = -k \times T \times \ln[\Xi(P,T,x)] \quad (2)$$

192 where: k =Boltzmann constant; st =lattice static contribution; vib =vibration contribution;
193 $Z(x,\Lambda)_{vib}$ =partition function from harmonic approximation for a given Λ -configuration;
194 $H(x,\Lambda)$ =enthalpy for a given Λ -configuration; $U(x,\Lambda)_{st}$ = lattice static energy for a given Λ -
195 configuration. Numerical calculations show that $Z(x,\Lambda)_{vib}$ exhibits, on average, a moderate
196 dependence on the Mg/Fe configuration. Therefore $Z(x,\Lambda)_{vib}$ of eq.(1) can be replaced with $Z(x)_{vib}$,
197 namely $\langle Z(x,\Lambda)_{vib} \rangle_{\Lambda=1,n}$ (see Section 3.2). From eq.(2) the Gibbs free energy can be split into two
198 parts: $G(x) = G(x)_0 + G(x)_{vib}$, where $G(x)_0$ collects the static contributions and $G(x)_{vib} = -$
199 $k \times T \times \ln(Z(x)_{vib})$. Transferring all this to the Gibbs energy of mixing (Ottonello 1997), we obtain:

$$200 \quad \Delta G(x)_{mixing} = \Delta G(x)_{0,mixing} + \Delta G(x)_{vib,mixing}.$$

201 where

$$202 \Delta G(x)_{0,mixing} = -k \times T \times \ln \left\{ \sum_{\Lambda=1,n} \exp[-(\Delta U(x, \Lambda)_{st,mixing} + P \Delta V(x, \Lambda)_{st,mixing}) / kT] \right\}. \quad (3)$$

203 Δ in eq.(3) means, for a generic thermodynamic “A” quantity of a mixing, the following difference:

$$204 \Delta A(x)_{mixing} = A(x) - x \times A(\text{FeO}) + (1-x) \times A(\text{MgO}).$$

205 According to Merli et al.(2015), the sum of eq.(3) can be approximated, so that

$$206 \Delta G(x)_{0,mixing} \approx -k \times T \times \ln[\xi(P, T, x)] - R \times T \times \ln(N(x)_{\text{configurations}}), \quad (4)$$

207 where: R is the gas constant; $N(x)_{\text{configurations}} = N_{\text{Avogadro}}! / \{ [x \times N_{\text{Avogadro}}]! [(1-x) \times N_{\text{Avogadro}}]! \}$;

$$208 \xi(P, T, x) = (1/N_{\text{sampled configurations}}) \times \sum_{\Lambda=1, \text{sampled configurations}} \exp[-(\Delta U(x, \Lambda)_{st,mixing} + P \Delta V(x, \Lambda)_{st,mixing}) / kT].$$

209 The subscript ‘sampled configurations’ means that the sum over *all* the possible configurations
210 ($\approx 10^{23}$, for 1 mole) is replaced with a random sampling over an appropriately chosen number of
211 different Fe/Mg arrangements for a given composition, *i.e.* $N_{\text{sampled configurations}}$.

212

213 3.2 Vibrational contributions to the Gibbs free energy of mixing

214

215 Semi-empirical potentials (Lewis and Catlow 1985; Merli et al., 2015), harmonic model and lattice
216 dynamics (GULP code; Gale 1997) were used to calculate $\Delta G(x)_{vib,mixing}$, from random Mg-Fe
217 configurations in 64 cation-sites super-cells over the **subsolidus** MgO-FeO binary. The range 30-70
218 GPa and 2000-3500 K was investigated for x -values strewn over the 0-1 interval, sampling up to
219 10^5 independent configurations. Attention was focussed on how mixing affects $\Delta G(x)_{vib,mixing}$. It was
220 observed that the $G(x, \Lambda)_{vib}$ -values oscillate, as a function of the random Λ -configurations, less than
221 0.1% around $G(x)_{vib}$, *i.e.* their Λ -average, which therefore provides a faithful estimate of the actual
222 vibrational contribution to the Gibbs energy for a given x . $\Delta G(x)_{vib,mixing}$, calculated accordingly,
223 amounts at most to about 2% of the configuration entropy contribution. **Given that in the present**
224 **case the harmonic $\Delta G(x)_{vib,mixing}$ contribution is very modest, then the anharmonic one is expected to**

225 be negligible. Altogether, P seems to make the vibrational contribution to the Gibbs energy of
 226 mixing of marginal importance for (Mg,Fe)O. Neglecting $\Delta G(x)_{vib,mixing}$ at high pressure is in
 227 contrast to what observed at room conditions (Merli et al., 2015), where a small, but significant
 228 vibrational contribution (10-15%) participates in the Gibbs energy of mixing.

229

230 3.3 Cluster expansion

231

232 $\Delta U(x, \Lambda)_{st,mixing} + P\Delta V(x, \Lambda)_{st,mixing}$ was computationally modelled exploiting the formalism that relies
 233 upon the cluster-expansion (Yuge 2010) and discrete Chebyshev polynomials (Merli et al. 2015;
 234 Sanchez et al. 1984). Such an approach leads to the following expression for $\Delta U(x, \Lambda)_{st,mixing} +$
 235 $P\Delta V(x, \Lambda)_{st,mixing}$ of a given Λ -configuration:

$$236 \Delta U(x, \Lambda)_{st,mixing} + P\Delta V(x, \Lambda)_{st,mixing} \approx \Delta H(P)_0 + \Delta H(P)_1 \times x + x \times (1-x) \times [A(P)_0 + A(P)_{Fe \times x}] +$$

$$237 \sum_{j=1, \text{number of clusters}} A(P)_{Fe-Mg,j} \times n(x, \Lambda)_{Fe-Mg,j}, \quad (5)$$

238 This equation accounts for a Vegard-like residue; $A(P)_0$ and $A(P)_{Fe}$ contribute to a composition
 239 dependent parabolic term; $A(P)_{Fe-Mg,j}$ s weigh the number of Fe-Mg couples, *i.e.* $n(x, \Lambda)_{Fe-Mg,j}$, whose
 240 atoms are d_j apart from one another, and constitute the j^{th} -cluster. $\Delta H(P)_j$ and $A(P)_k$ are functions of
 241 the pressure and were modelled by polynomials like

$$242 \omega_j^{(0)} + \omega_j^{(1)} \times P^{v(j)} + \omega_j^{(2)} \times P^{\chi(j)} + \dots \quad (6)$$

243 The χ, v, \dots exponents for each j -coefficient were determined by a trial-and-error approach,
 244 whereas the $\omega_j^{(0,1,2,\dots)}$ -coefficients were obtained by fitting the expression given by eq.(5) to the
 245 values calculated by quantum-mechanics. Preliminary tests indicated that parabolic expansions are
 246 appropriate for eq.(6); adding higher order terms does not enhance the quality of the results.
 247 Eventually, using eq.(5) and (6), $\xi(P, T, x)$ of eq.(4) was calculated by sampling $\sim 10^6$ - 10^8 Λ -
 248 configurations (Merli et al. 2015), which guarantee negligible oscillations of the resulting
 249 $\Delta G(x)_{0,mixing}$.

250

251 **3.4 Ab- initio calculations**

252

253 Static enthalpy calculations and structure relaxation were carried out at a given 0 K pressure by the
254 HF/DFT-CRYSTAL14 program (Dovesi et al. 2009), which implements “*Ab-initio* Linear-
255 Combination-of-Atomic-Orbitals” in the case of periodic systems. Pressure was corrected for zero
256 point and thermal contribution following Merli et al (2016). A Hamiltonian based on the WC1LYP
257 functional (Scanavino et al. 2012; Scanavino and Prencipe 2013) was used in the present work,
258 along with the flexible HF-DFT hybrid scheme earlier discussed and adopted for (Mg,Fe)O at room
259 pressure by Merli et al. (2015). It relies upon mixing HF and DFT exchange energy contributions,
260 in terms of a Hartree-Fock fraction (\mathfrak{F}_x) given by $\mathfrak{F}_x=(1-x)\times\mathfrak{F}_{\text{MgO}}+x\times\mathfrak{F}_{\text{FeO}}+x\times(1-x)\times\mathfrak{F}_{\text{MgO}}\times\mathfrak{F}_{\text{FeO}}$
261 (hybridization, tuning of functional and delocalization error: Autschbach and Srebro, 2014;
262 Alfredsson et al. 2004). For the end-members the following hybridization rates were used:
263 $\mathfrak{F}_{\text{FeO}}=0.16$ (HS; calibration on the band gap) and 0.24 (LS; calibration on the HS to LS transition at
264 40 GPa, for $x=0.2$); $\mathfrak{F}_{\text{MgO}}=0.2$ (calibration on the band gap). Such an approach has proven effective
265 to yield mixing energies that are weakly sensitive to change of the end members’ hybridization rate.
266 Tests performed at room pressure show that shifts even by 30-35% of $\mathfrak{F}_{\text{MgO-FeO}}$ lead to mixing
267 enthalpy average changes within 5-10%. The following values were used for the tolerance
268 governing the accuracy of the integrals of the self-consistent-field-cycles: 10^{-6} for coulomb overlap,
269 10^{-6} for coulomb penetration, 10^{-6} for exchange overlap, 10^{-6} for exchange pseudo-overlap in direct
270 space, 10^{-12} for exchange pseudo-overlap in reciprocal space and 10^{-9} a.u. threshold for SCF-cycles’
271 convergence. The Mg basis set from Causà et al. (1986) was extended by the addition of diffuse *sp*
272 and *d* shells (85-11G* contraction). The O basis set of Ottonello et al. (2010) was used, modified by
273 the introduction of a *d* shell (84-11G* contraction) according to Belmonte et al. (2014). The Fe
274 basis set is from Valerio et al. (1995). The ability to reproduce physical observables of MgO and
275 FeO using the present computing set-up is discussed by Merli et al. (2015-2016).

276 The static contributions to the Gibbs free energy of the substance at 4-6 independent Λ -
 277 configurations were calculated using super-cells of 16 cation sites to obtain multiplicity-weighted
 278 average $\Delta U + P\Delta V$'s for each LS-composition of $x \sim 0.125-0.25-0.375-0.5-0.625-0.75-0.875$, at 24-
 279 40-70-90-110-128 GPa. The HS-state was treated alike, but restricting calculations to $x \sim 0.125-$
 280 $0.375-0.50-0.75-0.875$, at 24-60-80-110 GPa. The approach of Merli et al. (2015) was followed to
 281 model a HS-paramagnet, by resorting to disordered up and down spin configurations such as yield a
 282 total residual spin of zero.

283 The average $(\Delta U + P\Delta V)$ -values were then fitted by polynomials in x to get by interpolation
 284 additional $(\Delta U + P\Delta V)$ -values, strewn over the 0-1 x -range, at every explored P . Eq.(5-6) were
 285 eventually fitted to the obtained set, using average $n(x)_{\text{Fe-Mg,j}} = \langle n(x, \Lambda)_{\text{Fe-Mg,j}} \rangle_{\Lambda}$ calculated over 10^5 -
 286 configurations for each given x . A cut-off of 10 Å was chosen after tests to fix up the size of the
 287 clusters of expansion (5). By means of the $\Delta H(P)_k$ and $A(P)_j$ coefficients, the static term
 288 $\Delta U(x, \Lambda)_{st, mixing} + P\Delta V(x, \Lambda)_{st, mixing}$ was calculated for super-cells of 1024 Fe/Mg-atoms, and thereby
 289 $\Delta G(x)_{0, mixing}$ was determined according to eq.(4).

290 Given the fact that the vibrational contributions are negligible, we introduce the following
 291 approximation: $\Delta G(x)_{mixing} \approx \Delta G(x)_{0, mixing}$ and hereafter use $\Delta G(P, T, x)_{mixing}$ to indicate the bulk
 292 Gibbs free energy of mixing at P - T conditions and x FeO, calculated accordingly.

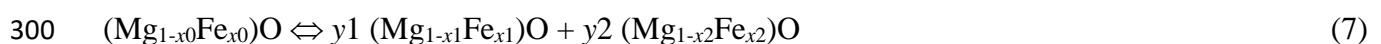
293

294 3.5 Reaction model

295

296 Once $\Delta G(P, T, x)_{mixing}$ is determined, it can be used to investigate the (Mg,Fe)O mixture at subsolidus
 297 and its interactions with the *reservoir* through irreversible disequilibrium reactions, implying an
 298 exchange of matter between *reservoir* and Fe-periclase.

299 We start from the basic reaction:



301 where x_i is the i^{th} FeO fraction, and y_i is the i^{th} phase fraction related to the Fe-periclase having x_i
302 FeO. To fulfil the mass conservation principle, y_1 and y_2 of eq.(7) result in (see Appendix I, for
303 derivation):

$$304 \quad y_1 = (x_0 - x_2) / (x_1 - x_2) \quad (8.a)$$

$$305 \quad y_2 = 1 - y_1. \quad (8.b)$$

306 Reaction (7) is dealt with from two points of view: one related to a *closed system*, and another to an
307 *open system*.

308 A *closed system* is modelled in terms of a given (Mg,Fe)O-phase that can *un-mix* into two more
309 stable compositions, according to the MgO-FeO binodal/spinodal curves (Ottonello 1997; for
310 application to the MgO-FeO system at room pressure see Merli et al 2015). *Un-mixing is intimately*
311 *linked to the Gibbs energy minimization under the constraint of equality of chemical potentials.*
312 The *consolute* temperature, T_C , defines the upward limit of a miscibility gap in a T - X Schreinemaker
313 projection, *i.e.* the temperature above which un-mixing processes do not occur, for a given P , and
314 solid mixings are stable.

315 Alternatively, an *open system* is modelled, treating eq.(7) in terms of forward and backward
316 reactions, in which the left- and right-hand side members act both as reagents and products and
317 equilibrium is achieved when forward and backward rates are equal to one another. Eq.(7) is a
318 simplification of the possible more complex natural reactions involving a larger number of reactants
319 and products. x_0 is a 'reference *pivot*-composition', which is supposed to exist at any P - T point of
320 both LM and LLM geotherms, along with the compositions given by x_1 and x_2 (Appendix II). The
321 x_0 -value can be taken over the interval 0.15-0.20 FeO, since: (i) this range includes the average FeO
322 content of Fe-periclase inferred by the geochemical model (Table 1); (ii) it accounts for the most
323 frequent Fe-periclase's compositions observed both in natural findings from lower mantle samples
324 (Harte, 2010; Kaminsky, 2012) and in Fe/Mg partitioning experiments (Auzende et al., 2008;
325 Nakajima et al., 2012; Prescher et al., 2014). In this model, the (Mg,Fe)O-system achieves P - T - X
326 equilibrium with a thermodynamic matter *reservoir*, which behaves as an ideal Fe/Mg exchanger

327 (see Appendix II and III for a description of the disequilibrium-to-equilibrium process, involving
 328 Fe-periclase and *reservoir*). Such a matter *reservoir* is the portion of lower mantle other than Fe-
 329 periclase and can be likened, in terms of *bare* MSF-composition, to a “virtual” (Mg,Fe)-perovskite
 330 (Table 1).

331 The phase proportions of the solid mixings that correspond to the x_0 -, x_1 - and x_2 -compositions are
 332 addressed here by means of λ_0 , λ_1 and λ_2 , respectively. Note that

$$333 \lambda_0 + \lambda_1 + \lambda_2 = 1. \tag{8.c}$$

334 The equilibrium constant of the reaction (7) is

$$335 K(P, T, x_0, x_1, x_2) = \exp[-(\Delta G(P, T, x_0)_{\text{mixing}} - y_1 \times \Delta G(P, T, x_1)_{\text{mixing}} - y_2 \times \Delta G(P, T, x_2)_{\text{mixing}}) / RT] \approx$$

$$336 \lambda_0 / (\lambda_1^{y_1} \times \lambda_2^{y_2}), \tag{9}$$

337 where the activity coefficient is approximated by unity.

338 For each $\{x_0-x_1-x_2\}$ -set we seek for the $\{\lambda_0, \lambda_1, \lambda_2\}$ -set that minimises the function

$$339 \Delta G(P, T, x_0, x_1, x_2)_{\text{Totalmixing}} = \lambda_0 \times \Delta G(P, T, x_0)_{\text{mixing}} +$$

$$340 \lambda_1 \times \Delta G(P, T, x_1)_{\text{mixing}} + \lambda_2 \times \Delta G(P, T, x_2)_{\text{mixing}}, \tag{10}$$

341 under the constraints given by eq.(8.a-b-c and 9).

342 Such an approach implies that:

343 (i) an exchange of FeO/MgO between (Mg,Fe)O-system and lower mantle *reservoir* takes place *via*

344 $\lambda_0 - \lambda_1 - \lambda_2$ under the sole constraint that the global bulk (FeO+MgO) content must be preserved, so

345 that Fe-periclase gives Δx -moles of FeO(MgO) to the *reservoir* and takes as many moles of

346 MgO(FeO) from it;

347 (ii) the point above requires that the incorporation of FeO/MgO into the *reservoir* causes variations

348 of its Gibbs energy that are assumed of the same order of magnitude of the oscillations occurring

349 because of the many reactions in the lower mantle (Appendix III). Such an assumption is equivalent

350 to taking Fe-periclase as the pivot-exchanger for iron/magnesium in the deep interior of the Earth.

351 This is consistent with that the Fe/Mg partitioning coefficient between bridgmanite (the other main

352 mineral competitor for incorporation of Fe) and Fe-periclase is observed to be significantly smaller
 353 than 1, *i.e.* (Mg,Fe)O is the main host of iron.

354 The λ_j -values, determined according to eq.(9-10), depend on x_0 , x_1 , x_2 , P and T , so that $\lambda_j(x_0, x_1,$
 355 $x_2)$, dropping for brevity P and T . Given that we are interested in average values, mean phase
 356 proportions, $\langle \lambda_j \rangle$, were obtained by a numerical integration over the allowed x_0 , x_1 and x_2 ranges
 357 (note that $x_2 < x_0 < x_1$, due to that $0 < y_1 < 1$), that is:

$$358 \quad \langle \lambda_j \rangle = C \int_{x_0-inf}^{x_0-sup} dx_0 \int_{x_0}^1 dx_1 \int_0^{x_0} \lambda_j(x_0, x_1, x_2) dx_2 \quad (11)$$

359 where C is a normalization factor, $x_0-sup=0.20$ and $x_0-inf=0.15$.

360 $\langle x_0 \rangle$, $\langle x_1 \rangle$ and $\langle x_2 \rangle$ are calculated as $\langle \lambda_j x_j \rangle / \langle \lambda_j \rangle$. This way, $\langle \lambda_{0,1,2} \rangle$ and $\langle x_{1,2} \rangle$ depend on
 361 P - T only, and show how the (Mg,Fe)O-system changes along a pressure-temperature path in terms
 362 of Mg-Fe-solid mixings. Note that eq.(7) and integration x_0 -interval imply that $\langle x_0 \rangle$ is equal to
 363 0.175.

364 In the ensuing discussions, the notations x_j (j^{th} -phase's composition) and λ_j (j^{th} -phase proportion)
 365 will be used in place of $\langle x_j \rangle$ and $\langle \lambda_j \rangle$ from eq. (11), for simplicity.

366

367 **3.6 Spin state and excess Gibbs energy of mixing**

368

369 LS-HS mixed states, which affect the physical properties of the (Mg,Fe)O-phases, are often
 370 accounted for in a solid mixing by a linear combination of the pure LS and HS systems (Lyubutin et
 371 al., 2009; Wentzcovitch et al. 2009; Muir and Brodholt, 2015; Vilella et al., 2015). It is
 372 straightforward to prove that in a HS-LS-(FeO-MgO) system (x^{LS-HS} - x^{LS} - x^{HS} being x - FeO in mixed
 373 HS-LS state, pure LS or HS state, respectively) the exact mixing energy is expressible as

$$374 \quad \Delta G(P, T, x^{LS-HS})_{mixing} = \eta \times \Delta G(P, T, x^{LS})_{mixing} + (1-\eta) \times \Delta G(P, T, x^{HS})_{mixing} +$$

$$375 \quad \{G(P, T, x^{LS-HS}) - \eta \times G(P, T, x^{LS}) - (1-\eta) \times G(P, T, x^{HS})\}, \quad (12)$$

376 where $\eta = 1/(1+\exp((G^{LS}-G^{HS})/xRT))$. In principle, it is possible to calculate the quantity $G(x^{LS-}$
 377 $^{HS},P,T)$, but in practice it is difficult, because of the exceedingly large super-cell size required in
 378 order to achieve statistical representativeness and faithfulness, and of the many configurations to
 379 explore. However, if we assume that the third term of the right-hand side member of the eq.(12) is
 380 negligible, then the equilibrium constant, *i.e.* eq.(9), becomes:

$$\begin{aligned}
 381 \quad K(P,T,x_0,x_1,x_2) &= \exp[-\eta \times \Delta G(P,T,x_0,x_1,x_2)^{LS}_{mixing}/RT] \times \exp[-(1-\eta) \times \Delta G(P,T,x_0,x_1,x_2)^{HS}_{mixing}/RT] \approx \\
 382 \quad & [K(P,T,x_0,x_1,x_2)^{LS}]^\eta \times [K(P,T,x_0,x_1,x_2)^{HS}]^{(1-\eta)} = \\
 383 \quad & \{[\lambda_0/(\lambda_1^{y_1} \times \lambda_2^{y_2})]^{LS}\}^\eta \times \{[\lambda_0/(\lambda_1^{y_1} \times \lambda_2^{y_2})]^{HS}\}^{(1-\eta)} \quad (13)
 \end{aligned}$$

384 where two sets of ‘‘virtual’’ phase proportions of the x_0 -1-2-phases are defined, *i.e.* $[\lambda_0, \lambda_1, \lambda_2]^{LS}$
 385 and $[\lambda_0, \lambda_1, \lambda_2]^{HS}$. LS and HS can be treated as decoupled states, with respect to the constraint
 386 given by eq.(13). Although such approximation provides an ‘‘extreme’’ depiction, as only pure spin
 387 states are involved, it gives a general view of how far either spin state affects the reactivity of the
 388 (Mg,Fe)O-system and guarantees the required precision to treat small and complex quantities such
 389 as mixing energy.

390 Using the cluster expansion technique (see section 3.3), we generated $\Delta G(P,T,x)_{mixing}$ data for either
 391 iron state and interpolated them by Redlich-Kister-type expressions (Stølen and Grande 2004),
 392 which model the mixing Gibbs energy as

$$393 \quad \Delta G(P,T,x)_{mixing} = x \times (1-x) \times h(P,T,x) + R \times T \times [x \times \ln(x) + (1-x) \times \ln(1-x)],$$

394 where the first term of the right-hand side member gives the excess enthalpy, and

$$395 \quad h(P,T,x) = \sum_{l=0,L,m=0,M;n=0,N} p_{lmn} \times P^l \times T^m \times x^n$$

396 The p_{lmn} -parameters of the expansion above for LS and HS (interval: $x=0-1$, $T=1900-4000$ K, $P=24-$
 397 140 GPa) are reported in Table 2.

398

399 4. RESULTS

400

401 **4.1 Un-mixing processes in closed (Mg,Fe)O-system**

402

403 Our calculations predict that at lower mantle P - T conditions, HS never gives rise to un-mixing
404 reactions in the MgO-FeO system at subsolidus, as $T_C < T_{\text{geotherms}}$ (Fig.1). LS, too, yields T_C values
405 that are smaller than the temperatures of both LM and LLM geotherms (Fig.1), but for the
406 shallowest portions of the lower mantle (~23-42 GPa). Pure LS gives un-mixings between 0.24 and
407 0.84 FeO (Fig.2), at the base of the immiscibility region ($T_C = 1920$ K, $P = 24$ GPa), and between
408 0.50 and 0.65 FeO, at its top ($T_C = 2174$ K, $P = 42$ GPa). Given that for reference Fe-periclase
409 composition, HS on average prevails up to ~40 GPa (Fei et al. 2007; Lin et al. 2007) and stabilizes
410 solid mixings (Fig.1), it is unlikely that the un-mixed products due to LS can provide an important
411 contribution in nature below ~40 GPa.

412 It is important to note that almost all the experiments agree to exclude that Fe-periclase un-mixes at
413 lower mantle conditions. Lin et al. (2003) and Ohta et al. (2014), who explored the compositional
414 range from 0.61 to 0.95 FeO, did not observe any disproportionation, except for *quasi*-wüstite
415 compositions (140 GPa-2580 K). Conversely, Dubrovinsky et al. (2000; 2001) report un-mixing of
416 (Mg,Fe)O, with x up to about 0.5 FeO, into Mg-rich and Fe-rich periclase like phases, but at
417 conditions far from lower mantle's (86 GPa and 1000 K). However, the relevant variety of Fe-
418 periclase compositions observed in the lower mantle diamond inclusions (Kaminsky, 2012 and
419 reference therein) and in the samples from Fe/Mg bridgmanite/Fe-periclase partitioning experiments
420 (Auzende et al., 2008; Nakajima et al., 2012; Prescher et al., 2014) has to be explained.

421

422 **4.2 Extension to the MgO - FeO - SiO₂ system**

423

424 The wide range of Fe-periclase compositions (the statistically most relevant interval is ~0.3-0.5
425 FeO) observed both in natural findings and in HP-HT syntheses suggests that the (Mg,Fe)O-system

426 can be modelled by reactions according to eq. (7), which imply forward-backward transformations
427 and may include exchange of matter with the surroundings.

428 Fig. 3a and 3b show x_j and λ_j as function of P , along the lower mantle geotherms, for LS and HS.
429 All the compositions exhibit slight changes (not graphically appreciable) in the case of HS over the
430 explored P range (Fig.3a), whereas a significant enrichment in Fe occurs in the x_1 -phase for LS.
431 The phase proportions of the x_0 -, x_1 - and x_2 -phases (Fig. 3b) remarkably vary along the geotherms
432 in the case of LS, only.

433 $\langle K(P,T) \rangle$ as function of P (Fig.4a), namely the average equilibrium constant obtained by an
434 integration over the allowed x_0 - x_1 - x_2 ranges of eq.(7), provides a partial explanation for the
435 insensitivity to P - T of the HS's λ -values (Fig.3b). In fact, LS exhibits a significantly steeper trend
436 than HS, along the LM-LLM-paths ($\partial \langle K(P,T) \rangle / \partial P \approx 9 \cdot 10^{-4}$ and $2 \cdot 10^{-4}$ GPa⁻¹, for LS and HS,
437 respectively), suggesting that different mixing behaviours take place as a function of the spin state.

438 The average equilibrium constant for HS is, in practice, *quasi*-invariant over the LM and LLM
439 mantle regions (Fig. 4a). In addition, the LS-HS excess enthalpy functions (ΔH_{excess}), at 24/1900-
440 107/2910 GPa/K, show relevant differences (Fig. 4b). LS has larger absolute ΔH_{excess} and
441 $d\Delta H_{\text{mixing}}/dx$ values than HS; this underlies that the LS (Mg,Fe)O-system is more sensitive to P - T in
442 terms of equilibrium constant than HS. LS and HS exhibit excess enthalpy curves similar in shape
443 at 24 GPa, but they remarkably change at 107 GPa, in such a way that the two spin states yield
444 opposite trends (Fig.4b).

445

446 5. DISCUSSION

447

448 On the basis of these results, LS can be consider the main booster of phase changes in the
449 (Mg,Fe)O-system over most of the LM and LLM regions. Therefore, we focus on the results of the
450 LS-state only.

451 The x_2 -phase (FeO \sim 0.10, at 24 GPa) mimics the x_0 -phase (FeO \sim 0.175 as inferred by the bulk
452 geochemical model), showing slight changes in composition along the geotherms (Fig. 3a). This
453 implies that both x_2 =Mg₉₀Fe₁₀-phase and, obviously, x_0 =Mg₈₂Fe₁₈-reference-phase are products in
454 the (Mg,Fe)O-system, which occur at any P - T of the lower mantle regions.

455 Conversely, the x_1 -phase [(Mg_{0.61}Fe_{0.39})O at 24 GPa] remarkably changes in composition with
456 respect to both x_0 and x_2 , increasing over the entire LM region (up to \sim 80 GPa) its Fe-content up
457 to 0.49 (Fig. 3a). This leads to an enrichment of 0.1 FeO from 24 to 80 GPa; at higher pressure
458 (LLM region), the x_1 -phase stabilises at \sim 0.5 FeO content (Fig. 3a).

459 At 24 GPa, the x_0 - x_1 - x_2 -phases occur in proportions of $\lambda_0 \approx 0.34$, $\lambda_1 \approx 0.23$ and $\lambda_2 \approx 0.43$ (Fig.3b),
460 respectively. The iron rich x_1 -phase is the least abundant in the uppermost part of the lower mantle,
461 but rapidly increases exceeding x_0 - and x_2 -phases at some 30 GPa, along the LM geotherm. At 80
462 GPa (\sim 2000 Km depth), the x_1 -phase, (Fe_{0.5}Mg_{0.5})O, reaches the proportion of \sim 0.67. Deeper, in
463 the region of the LLM geotherm (80-130 GPa), the iron rich x_1 -phase keeps on being the most
464 abundant reaction product in the (Mg,Fe)O-system (Fig.3b). This suggests that the modelled
465 possible products of the (Mg,Fe)O-system in the LLM region are highly stable, invariant in
466 composition and proportion.

467 Moreover, we observe that the x_1 -phase is the major exchanger with the *reservoir*; this is consistent
468 with the fact that the x_1 -composition is the most distant among x_0 -1-2-phases' from *reservoir*'s,
469 thus suggesting the occurrence of elemental concentration gradients that promote flow of matter. In
470 turn, the x_2 -phase's comparatively low amount might be related to a high activation energy to
471 achieve the critical size of nucleation that triggers then crystal growth.

472 As expected, the density (ρ) of the x_0 - x_1 - x_2 -phases progressively increases as function of P (Fig.5).
473 At 24 GPa, the most dense x_1 -phase [(Fe_{0.39}Mg_{0.61})O; ρ_{x_1} =5.3 g/cm³] is also the least abundant
474 (Fig.3b), whereas the x_0 - and x_2 -phases, which share almost equal density values (4.6 and 4.3
475 g/cm³, respectively), together account for \sim 0.80 phase proportion in the (Mg,Fe)O-system (Fig.3b;
476 Fig.5). Consequently, the average density of the (Mg,Fe)O-system in the shallow part of the lower

477 mantle (~700 Km) is controlled by iron poor phases (~4.5 g/cm³). It is worth noting that the density
478 of the x_1 -phase increases linearly in the LLM region, even if the x_1 -phase ceases to incorporate
479 additional iron from the *reservoir* at about 80-90 GPa. This implies that below ~2000 Km depth, the
480 bulk density of the (Mg,Fe)O-system (6.5 g/cm³, using the LLM geotherm), primarily depends on
481 the pure physical properties of the involved phases, which are invariant in composition and phase
482 fractions from ~90 GPa to the core-mantle boundary. Moreover, if the (Mg,Fe)O-system is
483 considered as constituted by x_1 and (x_0+x_2) only, then they yield a net change in terms of
484 differential density, *i.e.* $\Delta\rho=[\rho_{x_1} -(\rho_{x_0} +\rho_{x_2})\times 0.5]$, from 0.8, at 24 GPa, to 1.4, at 130 GPa. This
485 corresponds altogether to a mean $\Delta\rho$ -increase of approximately 10%, in keeping with the results of
486 Rost et al. (2005) and McNamara et al. (2010).

487 On the whole, the lower mantle (Mg,Fe)O-system with the pyrolitic reference composition 0.175
488 FeO (Table 1) tends to acquire iron from the *reservoir* upon increasing pressure, for a maximum
489 *total* enrichment of ~0.22 FeO and by effect of LS only (Fig.6).

490 Following the suggestion of iron-rich starting material used in a few Fe/Mg periclase/bridgmanite
491 partitioning experiments (Nakajima et al., 2012), a fictitious 'not-pyrolitic' lower mantle (Fe,Mg)O-
492 system with a reference composition $x_0=0.3$ FeO was also modelled, in order to test the sensitivity
493 of eq.(7) to x_0 in the case of LS. This system results in a weaker exchanger with the *reservoir*
494 (≤ 0.09 Fe at ~130 GPa) in comparison with the pyrolitic model, and the compositions of the
495 resulting phases scarcely change along both the LM and LLM P - T paths. The Fe-rich phase occurs
496 with ~0.55 FeO at 24 GPa, ~0.51 FeO at 48 GPa and then slightly increases its iron content to ~0.52
497 FeO at ~130 GPa. These data reflect an iron-saturation effect in the (Mg,Fe)O-system, owing to an
498 unduly large x_0 -value for the reference composition with respect to the pyrolitic model (Table 1,
499 Fig. 3).

500 For the sake of completeness, it is worth pointing out that a simultaneous occurrence of LS and HS
501 depicts the most likely Earth's lower mantle iron state (Lin et al., 2013). We approximately
502 estimated the LS-HS effects by linearly combining the results from one spin state with those of the

503 other using the η -weighting function (see eq.13). In so doing and leaving aside any claim of
504 precision, the composition of the x_1 -mixed-states-phase achieves the same "saturation" value as
505 for pure LS of 0.5 FeO upon P , at about 100 GPa. The general trends of the phases' compositions
506 and phase proportions in mixed spin states as a function of the geotherms are preserved with respect
507 to pure LS's, although they are shifted by ~ 20 GPa to higher P -values. Despite the level of
508 approximation we have to accept in view of the complexity of the reactions occurring in the lower
509 mantle, altogether our results corroborate that $(\text{Fe}_{0.5}\text{Mg}_{0.5})\text{O}$ -phase is expected to be the likeliest Fe-
510 rich periclase composition in the LLM region (from 80-100 GPa), independently of the x_0 -reference
511 composition. This is in agreement with the results of multicomponent experiments that, using as
512 starting material the San-Carlos olivine (0.3 FeO), yield Fe-periclase whose highest iron content is
513 0.487 FeO (Nakajima et al., 2012). We are aware that a direct comparison between theoretical and
514 experimental results has to be taken with due care. In fact, *HP-HT* experimental set-up, reaction
515 kinetics and compositional constraints significantly affect the results, causing deviations from
516 expectations (*i.e.* high temperature effects on transformations, occurrence of gradients, meta-
517 stability, complex REDOX-reactions).

518

519 **5.1 Fe/Mg partitioning between reservoir and Fe-periclase**

520

521 Using the *reservoir*'s composition (likened to a "virtual" bridgmanite's; Table 1) and the predicted
522 $(\text{Mg,Fe})\text{O}$ -phases, the bulk Fe/Mg partitioning between *reservoir* and Fe-periclase
523 [$\text{Kd} = (\text{Fe}/\text{Mg})^{\text{reservoir}} / (\text{Fe}/\text{Mg})^{\text{Fe-periclase}}$] was calculated. In this view, Kd may be considered as an
524 approximate estimate of the actual partitioning between bridgmanite and Fe-periclase, yet taking
525 into account that we are neglecting the *reservoir*'s energetics and therefore we assume that the
526 Fe/Mg exchange/equilibration is driven by the $(\text{Mg,Fe})\text{O}$ -system only, as already stated. Kd is
527 determined weighting the Fe-periclase x_0 - x_1 - x_2 -phases by their proportions.

528 In the LM region, when the LS state drives the degree of iron reactivity, a continuous decrease of
529 K_d from 0.64 to 0.19 can be observed. At higher pressures, in the LLM region, where the
530 (Mg,Fe)O-system's phases do not significantly change, neither in composition nor in proportion,
531 the bulk Fe/Mg- K_d is almost constant ($K_d=0.18-0.16$ between ~80 and 130 GPa). If the Fe/Mg
532 partitioning between *reservoir* and Fe-periclase is calculated treating each x_j -phase as independent
533 of the others, then K_d -intervals of 0.5-0.3, 0.18-0.06 and 1-0.5, for x_0 , x_1 and x_2 , respectively, are
534 obtained. This means that the (Mg,Fe)O-phases exhibit diverse attitudes to iron hosting.

535 In addition, if a mixed spin state of ferrous iron was taken into account, the K_d -values would
536 increase because of the HS contribution. However, using the compositions and phase proportions
537 obtained from HS-LS linear combination, the Fe-Mg partitioning trend does not change with respect
538 to LS's, with K_d -values as large as 0.19-0.16 in LLM region.

539 Our results of Fe/Mg partitioning between *reservoir* and Fe-periclase agree with experimental and
540 theoretical studies on pyrolitic and Al-free systems, which give K_d , for bridgmanite/Fe-periclase,
541 ranging from 0.6 to 0.06 (*i.e.* Deschamps and Trampert, 2004; Kobayashi et al., 2005; Sakai et al.,
542 2009; Auzende et al., 2008; Nakajima et al., 2012; Preshler et al., 2014; Miur and Brodhlt, 2016). In
543 particular, *HP-HT* experiments carried out between 30-130 GPa and 1760–2500 K (Preshler et al.
544 2014; Sinmyo et al. 2008, 2013; Narigyna et al., 2011) yield K_d -estimates showing a trend
545 flattening at LLM pressures like our predictions, although in a restricted range of values (0.35-0.16
546 *versus* 0.69-0.16). Taking into account that we modelled the Fe/Mg exchange/equilibration
547 neglecting the *reservoir*'s energetics, the general consistency between the present results and
548 previous determinations suggests that iron always prefers Fe-periclase in comparison to all the other
549 iron-bearing phases of the lower mantle.

550

551 **6. CONCLUSIONS**

552

553 To our knowledge, this is the first investigation which uses Gibbs energy of mixing, forward-
554 backward transformations and treats the (Mg,Fe)O system as an open exchanger of matter with the
555 lower mantle surroundings.

556 Un-mixings over the closed MgO-FeO binary at lower mantle P - T conditions are predicted to occur
557 between 23 and 42 GPa in the case of LS, only. Taking into account that HS is the preferred spin
558 state of iron up to ~40 GPa and that it excludes occurrence of disproportionation at any pressure,
559 un-mixing processes are therefore unlikely. In this light, it is difficult to ascribe to un-mixing
560 phenomena the observed compositional variability of lower mantle Fe-periclase in diamond
561 inclusions and in HP-HT synthesis products.

562 In turn, using a geochemically open model and equilibrium reactions formalism, we show that the
563 (Mg,Fe)O-system is able to continuously exchange iron with the lower mantle *reservoir* (*i.e.* MSF-
564 system) and provides the phases x_0 (reference average; 0.175 FeO), x_1 and x_2 . x_1 increases
565 progressively in phase proportion, becoming richer and richer in iron up to 0.5 FeO at ~80 GPa
566 (~2000 km depth). x_2 , 0.10 FeO, is *quasi*-invariant in composition and occurs with phase proportion
567 values that decrease as a function of P , similarly to x_0 's. Above ~80 GPa, such phases change
568 neither in composition nor in phase proportion, and the Fe-rich phase becomes the most abundant in
569 the LLM region, in terms of 0.7 phase proportion.

570 The resulting phases yield a larger and larger density inhomogeneity, estimated by $\Delta\rho=[\rho_{x_1}-$
571 $(\rho_{x_0}+\rho_{x_2})\times 0.5]$. $\Delta\rho$ changes from 0.8, at 24 GPa, to 1.4, at 130 GPa, and corresponds altogether to a
572 mean increase of approximately 10%.

573 The Fe/Mg partitioning between *reservoir* (roughly approximated by a “virtual” bridgmanite
574 chemical composition) and Fe-periclase, *i.e.* K_d , decreases in LM following its geotherm, but it
575 becomes *quasi*-constant in LLM. In fact, K_d varies from 0.64, at 24 GPa, to 0.19, at 80 GPa and
576 from 0.18, at ~90 GPa, to 0.16, at 130 GPa, in general agreement with previous theoretical and
577 experimental determinations in the case of actual bridgmanite and Fe-periclase. This suggests that
578 iron prefers Fe-periclase in comparison to all the other iron-bearing phases of the lower mantle.

579 In summary:

- 580 - the obtained results indicate the (Mg,Fe)O-system stabilises phases that ultimately give rise
581 to geochemical heterogeneities as a function of the P - T paths in LM and LLM. Such
582 heterogeneities are due to changes of the (Mg,Fe)O-phases in (i) composition, (ii) phase
583 proportions, (iii) density and (iv) Fe/Mg partitioning coefficients between *reservoir* and Fe-
584 periclase. These changes, which rapidly occur across LM, become significantly more
585 modest in LLM, where a steady Fe-rich-phase is dominant (~0.7 phase proportion);
- 586 - Fe-periclase behaves as the main “pivot” in the Fe/Mg-exchange processes with respect to
587 the lower mantle *reservoir*;
- 588 - (Mg,Fe)O is a source of geochemical heterogeneities (the average compositions from 24 to
589 130 GPa are strewn over the interval 0.19-0.40 FeO), but it does not give rise to any sharp
590 discontinuity. In this view, anomalies, like the ultra-low velocity zones (ULVZs),
591 interpreted as due to local abrupt change of density, do not seem primarily associated to the
592 mixing behaviour of Fe-periclase.

593

594 **ACKNOWLEDGEMENTS**

595

596 The present research was funded by the Italian University and Research Ministry (MIUR)
597 /PRIN2015_ project (CB). The authors are thankful to three anonymous reviewers and the
598 Associate Editor for their useful suggestions and remarks, which relevantly improved the original
599 manuscript.

600

601 **APPENDIX I**

602

603 **Derivation of equations (8.a) and (8.b)**

604

605 Starting from eq.(7), we require that the conservation of mass principle is fulfilled between right-
606 hand side and left-hand side members. Therefore, we have

$$607 \quad x_0 = y_1 \times x_1 + y_2 \times x_2 \quad (\text{I.1.a})$$

$$608 \quad 1 - x_0 = y_1 \times (1 - x_1) + y_2 \times (1 - x_2) \quad (\text{I.1.b}).$$

609 Summing (I.1.a) and (I.1.b), we obtain

$$610 \quad y_1 + y_2 = 1 \quad (\text{I.2})$$

611 Expressing y_2 in (I.1.a) by (I.2), we determine y_1 as a function of x_1 and x_2 , *i.e.* equation (8.a). Eq.
612 (8.b) is a consequence of (I.2).

613

614 APPENDIX II

615 Open system and constrained phase assemblages

616 With μ_j^α and n_j^α we represent the chemical potential and number of moles of the j^{th} -component with
617 respect to the α -phase, respectively. We assume the existence of one *independent* and *known* phase,
618 “ 0 phase”. Its composition is fixed and expressed by n_j^0 ; ξ stands for the number of moles of the
619 0 phase. The introduction of the 0 phase is needed when the complexity of a system is so high that a
620 further constraint on the nature of the involved phases can help addressing the problem. For
621 instance, such a situation is met when transformation kinetics is low, or impaired, and leads to the
622 persistence of one or more phases, which constrain the phase composition of the resulting
623 assemblage. Phases other than the 0 phase (they are here addressed to as *dependent* phases) are in
624 total p ; c indicates the number of components.

625 The Gibbs energy of such a system is

$$626 \quad G = \sum_{\alpha=1,p} \sum_{j=1,c} n_j^\alpha \mu_j^\alpha + \xi \sum_{j=1,c} n_j^0 \mu_j^0.$$

627 At given P - T conditions we have

$$628 \quad dG = \sum_{\alpha=1,p} \sum_{j=1,c} \mu_j^\alpha dn_j^\alpha + \sum_{j=1,c} n_j^0 \mu_j^0 d\xi, \quad (\text{II.1})$$

629 and at equilibrium $dG=0$. If we assume the conservation of mass principle for components, *i.e.*
 630 closed system, then c -constraints are required to be fulfilled, *i.e.*

631
$$\sum_{\alpha=1,p} dn_j^\alpha + n_j^0 d\xi=0. \quad (\text{II.2})$$

632 Using the Lagrange multipliers (ψ_j) method, we combine (II.1) and (II.2), so that

633
$$\sum_{\alpha=1,p} \sum_{j=1,c} \mu_j^\alpha dn_j^\alpha + \sum_{j=1,c} n_j^0 \mu_j^0 d\xi + \sum_{j=1,c} \psi_j (\sum_{\alpha=1,p} dn_j^\alpha + n_j^0 d\xi)=0.$$

634 Rearranging the terms of the equation above, we can write

635
$$\sum_{j=1,c} [\sum_{\alpha=1,p} (\mu_j^\alpha + \psi_j) dn_j^\alpha + (\mu_j^0 + \psi_j) n_j^0 d\xi]=0. \quad (\text{II.3})$$

636 (II.3) requires that

637
$$\mu_1^1 = \mu_1^2 = \dots = -\psi_1 = \mu_1^0 \quad (\text{II.4})$$

638

639
$$\mu_c^1 = \mu_c^2 = \dots = -\psi_c = \mu_c^0$$

640 The set of equations (II.4) leads to the well understood equality between chemical potentials of the
 641 same component in different phases.

642 In the general approach, there is not any imposed ⁰phase, hence we set it aside for the moment. A
 643 set of $c \times p$ unknown $\{x_j^\alpha\}$ -values, *i.e.* component fractions on which the chemical potentials depend,
 644 must be determined. In this way, the problem of the absolute amount of each component can be
 645 avoided. However, component fractions require more p -constraints of normalization, *i.e.* $\sum_{j=1,c} x_j^\alpha=1$,
 646 in addition to the $c \times (p-1)$ constraints due to (II.4). Hence, at given P and T , the classic
 647 relationship: $f_{\text{degrees of freedom}} = (p \times c) - c \times (p-1) - p = c - p$ is obtained.

648 In the case of the presence of an *independent* ⁰phase, the constraining equations of (II.4)-type are
 649 $p \times c$, given that the lagrangian multipliers are determined by μ_j^0 , *i.e.* $-\psi_j = \mu_j^0$. We now assume the
 650 system to be off equilibrium but, in order to evolve towards the equilibrium state, it exchanges
 651 matter with a *reservoir* according to an irreversible transformation, $dG_{\text{irrev}} < 0$, which, once reached,
 652 fulfills (II.4) and $dG=0$. Hence, the p dependent phases behave as an “*open system*” in the

653 equilibration process. Relaxing the constraint of conservation of mass, we have to seek for $c \times p$
654 unknown $\{n_j^\alpha\}$ -values, $n_j^\alpha \geq 0$, to fulfill the $c \times p$ constraint equations of (II.4)-type. In this view, the
655 problem is solvable and the solution is unique, there being as many variables as constraints, and the
656 independent 0 phase pivots equilibration of the p dependent phases.

657 We now aim to introduce more than one *independent* phase: p_{indep} -phases. First, they must be at
658 equilibrium with each other at P - T , namely they must satisfy the constraints of the Gibbs rule, *i.e.*
659 $p_{\text{indep}} \leq c$ and the equality of the chemical potentials. The ψ_i 's, determined by the chemical
660 potentials of the *independent* phases accordingly, lead to the $c \times p$ constraining equations. The $\{n_j^\alpha\}$ -
661 values that determine the p dependent phases are obtained by exploiting an exchange of matter with
662 the *reservoir*, as in the case of the 0 phase.

663 It is worth noting that the obtained assemblage represents the least Gibbs energy system compatible
664 with p_{indep} *independent* ($p_{\text{indep}} \leq c$) and p dependent phases. The assemblage of *dependent* phases, in
665 turn, must be as physically consistent as possible with the conditions following a relaxation of the
666 constraints of the imposed *independent* phases. In this view, $p \leq c$, for the *dependent* phases, too.

667 The application discussed in the text for Fe-periclase can be likened to the case in which the
668 ubiquitous x_0 -phase acts as an *independent* 0 phase, whereas x_1 and x_2 are two *dependent* phases. In
669 other words, the *system* is divided into two sub-*systems* (either fully consistent with the Gibbs rule)
670 one of which exchanges matter with a *reservoir* and in this way equilibration is achieved.

671

672 **APPENDIX III**

673 ***System (Fe-periclase) and reservoir***

674 The *reservoir* provides a simplified description of that portion of the lower mantle other than
675 (Mg,Fe)O. Let us suppose that at given P - T -conditions, *reservoir* and (Mg,Fe)O, with compositions
676 $X_{\text{reservoir}}$ and $X_{(\text{Mg,Fe})\text{O}}$, respectively, interact and exchange matter. If P and T are kept constant, the
677 *system* and the *reservoir* undergo an irreversible transformation towards a Gibbs energy minimum.

678 If the *reservoir* is *compositionally* likened to a fictitious “bridgmanite”, (Mg,Fe)SiO₃, we can
 679 envisage an exchange of matter between it and the *system* through the following reaction:



681 in which χ FeO is transferred from the *reservoir* to the Fe-periclase, and χ MgO does the opposite.

682 The Gibbs energy of the *reservoir* at P - T conditions composed by N -moles of a given chemical
 683 component, is represented by $G_R(P,T,N) \pm \Delta_f$, where Δ_f is the *reservoir*’s fluctuation that accounts
 684 for the energy, complex transformations, reactions, and flows of matter that take place in the lower
 685 mantle. For simplicity, we restrict to one chemical component our analysis and use

$$686 g_{\text{Sys}}(P,T,n)$$

687 to refer to the “instantaneous” Gibbs energy of a *system* (Fe-periclase), in which n defines a generic
 688 reference composition at P - T . “Instantaneous” Gibbs energy means the Gibbs energy of the *system*
 689 frozen off equilibrium. We take $G_R(P,T,N) \gg g_{\text{Sys}}(P,T,n)$ and their total Gibbs energy is

$$690 G_{\text{tot}}(P,T,N,n) = g_{\text{Sys}}(P,T,n) + G_R(P,T,N) \pm \Delta_f. \quad (\text{III.1})$$

691 At a given time, *system* and *reservoir* start to interact and exchange matter. The exchange of matter
 692 leads to

$$693 G_R(P,T, N-\chi) \pm \Delta_f$$

694 and

$$695 g_{\text{Sys}}(P,T, n+\chi).$$

696 From eq.(III.1), we aim at minimizing the following quantity, with respect to χ ,

$$697 \Delta_{\text{tot}} = G_{\text{tot}}(P,T,N-\chi,n+\chi) - G_{\text{tot}}(P,T,N,n) \pm \Delta_f, \quad (\text{III.2})$$

698 in which *system*+*reservoir* evolve through an irreversible change towards an equilibrium state.

699 Given that $|G_R(P,T, N-\chi) - G_R(P,T, N)| \ll \Delta_f$, owing to $\chi \ll N$ and, from statistical mechanics,

700 $\Delta_f \propto N^{1/2}$, then we can neglect the change of the *reservoir*’s Gibbs energy due to an exchange of

701 matter with the *system* with respect to the fluctuations’ contribution.

702 In this light, eq.(III.2) becomes

703 $\Delta_{tot} \approx [\pm\Delta_f]_{reservoir} + [-\mu(P,T,n+\chi)_{Sys}\cdot\chi + O_{Sys}(\chi^2)]_{system},$ (III.3)

704 Eq.(III.3) shows that if a super-system composed by *reservoir+system* is considered, then the *system*
705 alone can be considered, if its size is significantly smaller than the *reservoir*'s. Therefore,
706 exchanges of matter are mainly governed by the *system*, given that they do not affect the *reservoir*
707 more than its fluctuations do.

708 **REFERENCES**

709

710 Albarede, F., van der Hilst, R.D., 2002. Zoned mantle convection. *Philos. Trans. R. Soc. Lond.*

711 Ser.A, Math.Phys. Eng. Sci.360, 2569–2592. <http://dx.doi.org/10.1098/rsta.2002.1081>.

712 Alfredsson, M., Price, G.D., Catlow, C.R.A., Parker, S.C., Orlando, R. Brodholt, J.P., 2004.

713 Electronic structure of the antiferromagnetic B1-structured FeO. *Phys. Rev. B* **70**, 165111-

714 165116.

715 Andrault, D., Bolfan-Casanova, N., Lo Nigro, G., Bouhifd, M.A., Garbarino, G., Mezouar, M.,

716 2011. Solidus and liquidus profiles of chondritic mantle: Implication for melting of the Earth

717 across its history. *Earth Planet. Sci. Lett.*, 304, 251-259.

718 Autschbach, J., Srebro, M., 2014. Delocalization Error and “Functional Tuning” in Kohn–Sham

719 Calculations of Molecular Properties *Acc. Chem. Res.*, 2014, 47 (8), 2592–2602

720 Auzende, A.-L., Badro, J., Ryerson, F.J., Weber, P., Fallon, S., Addad, A., Siebert, J., Fiquet, G.,

721 2008. Element partitioning between magnesium silicate perovskite and ferropericlasite: new

722 insights into bulk lower-mantle geochemistry. *Earth Planet. Sci. Lett.* 269, 164–174.

723 Badro, J., Fiquet, G., Guyot, F., Rueff, J., Struzhkin, V.V., Vankò, G., Monaco, G., 2003. Iron

724 Partitioning in Earth’s Mantle: Toward a Deep Lower Mantle Discontinuity. *Science*, 300,

725 789-791

726 Barnard, R. W., Dahlquist, G., Pearce, K., Reichel, L., Richards K. C., 1998. Gram Polynomials

727 and the Kummer Function. *J. Approx. Theory* 94, 128–143.

728 Belmonte, D., Ottonello, G., and Vetuschi Zuccolini, M., 2014. Ab initio thermodynamic and

729 thermophysical properties of sapphirine end-members in the join $Mg_4Al_8Si_2O_{20}$ –

730 $Mg_3Al_{10}SiO_{20}$. *American Mineralogist* 99, 1449-1461.

731 Causà, M., Dovesi, R., Pisani, C., Roetti, C., 1986. Electronic structure and stability of different

732 crystal phases of magnesium oxide. *Physical Review B*, 33, 1308-1316.

733 Cordier, P., Amodeo, J., Carrez, P. (2012) Modelling the rheology of MgO under Earth's mantle
734 pressure, temperature and strain rates. *Nature*, 481, 177-180.

735 da Silva, C.R.S., Wentzcovitch, R.M., Patel, A., Price, G.D., Karato, S.I., 2000. The composition
736 and geotherm of the lower mantle: constraints from the elasticity of silicate perovskite. *Phys.*
737 *Earth Planet. Int.* 103-109.

738 de Koker, N., 2010. Thermal conductivity of MgO periclase at high pressure: Implications for the
739 D'' region. *Earth Planet. Sci. Lett.*, 292, 392-398

740 de Wit, R.W.L., Trampert, J., 2015. Robust constraints on average radial lower mantle anisotropy
741 and consequences for composition and texture. *Earth Planet. Sci. Lett.*, 429, 101-109.

742 Deschamps, F., Trampert, J., 2004. Towards a lower mantle reference temperature and composition.
743 *Earth Planet. Sci. Lett.* 222, 161–175. <http://dx.doi.org/10.1016/j.epsl.2004.02.024>.

744 Dill, K.A., Bromberg, S., Stigter, D., 2003. *Molecular Driving Forces: Statistical Thermodynamics*
745 *in Chemistry and Biology..* (1st edition). pp 665. New York: Garland Science.

746 Dobson, D.P., Brodholt, J.P., 2005. Subducted banded iron formations as a source of ultralow-
747 velocity zones at the core–mantle boundary. *Nature*434, 371–374.

748 Dovesi, R., Saunders, V.R., Roetti, C., Orlando, R., Zicovich-Wilson, C.M., Pascale, F., Civalleri,
749 B., Doll, K., Harrison, N.M., Bush, I.J., D'Arco, P., Llunell, M. 2009. CRYSTAL09 user's
750 manual. University of Torino, IT, Torino

751 Dubrovinsky, L. S., Dubrovinskaia, N. A., Saxena, S. K. , Annersten, H. , Hålenius, E. , H.
752 Harryson, Tutti, F., Rekhi, S., Le Bihan, T. 2000. Stability of ferropericlase in the lower
753 mantle. *Science* 289, 430– 432

754 Dubrovinsky, L. S., Dubrovinskaia, N. A., Annersten, H., Hålenius, E. , Harryson, H. 2001.
755 Stability of magnesiowüstites (Mg_{0.50}Fe_{0.50})O and (Mg_{0.80}Fe_{0.20})O in the lower mantle. *Eur. J.*
756 *Miner.* 113, 857-861.

757 Dziewonski, A., Anderson, D.L., 1981. Preliminary earth reference model. *Phys. Earth Planet.*
758 *Inter.*25, 297–356.

759 Fei W., Zhang L., Corgna A., Watson H., Ricolleau A., Meng Y., Prakapenka V., 2007, Spin
760 transition and equation of state of (Mg,Fe)O solid solutions. *Geophys. Res. Lett.* 34, L17307.

761 Fei, Y., Mao, H.-K., Shu, J., Hu, J., 1992. P-V-T equation of state of magnesiowüstite
762 (Mg_{0.6}Fe_{0.4})O. *Phys. Chem. Miner.* 18, 416– 422.

763 Frost, D.J, Myhill, R. (2016) Chemistry of the lower mantle. In: *Deep Earth: Physics and Chemistry*
764 *of the lower mantle and core, Geophysical Monograph 217.* Edited by Teresaki H. and Fischer
765 R.A. American Geophysical Union. John Wiley and Sons, Inc.

766 Gale J. D., 1997, GULP-a computer program for the symmetry adapted simulation of solids. *JCS*
767 *Faraday Trans.* **93**, 629-637.

768 Garnero, E. J., 2004, A new paradigm for Earth's core-mantle boundary, *Science*, 304, 834–836,
769 doi:10.1126/science.1097849.

770 Girard, J., Amulele, G., Farla, R., Mohiuddin, A., Karato, S. (2016) Shear deformation of
771 bridgmanite and magnesiowüstite aggregates at lower mantle conditions. *Science*, 351, 144-
772 147.

773 Harte B. (2010) Diamond formation in the deep mantle; the record of mineral inclusions and their
774 distribution in relation to mantle dehydration zones. *Mineralogical Magazine*, 189–215.
775 <http://dx.doi.org/10.1180/minmag.2010.074.2.189>.

776 Irifune, T., Shinmei, T., McCammon, C. A., Miyajima, N., Rubie D. C., Frost D. J., 2010. Iron
777 Partitioning and Density Changes of Pyrolite in Earth's Lower Mantle. *Science* **327**, 193-195.

778 Jackson I., 1998. Elasticity, composition and the temperature of the Earth's lower mantle: a
779 reappraisal, *Geophys. J. Int.* 134, 291–311.

780 Jackson, J M., Sinogeikin, S. V., Jacobsen, S.D. , Reichmann, H. J., Mackwell, S.J. Bass, J. D.
781 2006. Single-crystal elasticity and sound velocities of (Mg_{0.94}Fe_{0.06})O ferropericlase to 20 GPa.
782 *Journal of Geophysical Research* 111, B09203

783 Jacobsen, S. D., Spetzler, H., Reichmann, H.-J., Smyth, J. R., 2004. Shear waves in the diamond-
784 anvil cell reveal pressure-induced instability in (Mg,Fe)O. Proceedings of the National
785 Academy of Sciences of the United States of America, 101, 5867– 5871

786 Javoy M., Kaminski E., Guyot F., Andrault D., Sanlou J. R., Moreira M., Labrosse S., Jambon A.,
787 Agrinier P., Davaille A., Jaupart C., 2010. The chemical composition of the Earth: Enstatite
788 chondrite models. Earth Planet. Sci. Lett. 293, 259-268.

789 Kaminsky, F., Lin, J-F. (2017) Iron partitioning in natural lower-mantle minerals: toward a
790 chemically heterogeneous lower mantle. Am. Miner., DOI: [http://dx.doi.org/10.2138/am-2017-](http://dx.doi.org/10.2138/am-2017-5949)
791 5949.

792 Kaminsky, F., 2012, Mineralogy of the lower mantle: A review of ‘super-deep’ mineral inclusions
793 in diamond. Earth-Science Reviews, 110, 127–147

794 Kaneshima, S., Helffrich G., 1999. Dipping low-velocity layer in the mid-lower mantle: evidence
795 for geochemical heterogeneity. Science, 283, 1888–1891.

796 Karki, B. B., Wentzcovitch, R. M., de Gironcoli, S., Baroni, 2001. First principles thermoelasticity
797 of MgSiO₃-perovskite: consequences for the inferred properties of the lower Mantle. Geophys.
798 Res. Lett. 28, 2699-3702.

799 Kennett, B.L, Engdahl , E.R., Buland. R.,1995. Constraints on seismic velocities in the earth from
800 travel times. Geophys.J. Int. 122:108-124.

801 Kobayashi, Y., T. Kondo, E. Ohtani, N. Hirao, N. Miyajima, T. Yagi,T. Nagase, and T. Kikegawa
802 (2005), Fe-Mg partitioning between (Mg, Fe)SiO₃ post-perovskite, perovskite, and
803 magnesiowüstite in the Earth’s lower mantle. Geophys. Res. Lett., 32, L19301, doi:10.1029/
804 2005GL023257.

805 Kung, J., Li, B., Weidner, D. J., Zhang, J., Liebermann, R. C., 2002. Elasticity of (Mg_{0.83},Fe_{0.17})O
806 ferropericlase at high pressure: Ultrasonic measurements in conjunction with X-radiation
807 techniques. Earth Planet. Sci. Lett., 203, 557–566.

808 Kurnosov, A., Marquardt, H., Frost, D.J., Boffa Ballaran, T., Ziberna, L. (2017) Evidence for a
809 F3+-rich pyrolytic lower mantle from (Al,Fe)-bearing bridgmanite elasticity data. *Nature*, 543,
810 543-546.

811 Lay T., Helmberger D.V., 1983. A shear velocity discontinuity in the lower mantle. *Geoph. Res.*
812 *Lett.* 10, 63-66.

813 Lay, T., Garnero, E.J., Williams, Q., 2004. Partial melting in a thermo-chemical boundary layer at
814 the base of the mantle. *Phys. Earth Planet. Inter.* 146, 441–467.

815 Lewis, G. V., Catlow, C. R. A., 1985. Potential models for ionic oxides. *J. Phys. C: Solid State Phys.*
816 18, 1149-1162.

817 Li, L., Brodholt, J.P., Stackhouse, S., Weidner, D.J., Alfredsson, M., Price, G.D., 2005. Elasticity of
818 (Mg,Fe)(Si,Al)O₃ perovskite at high pressure. *Earth Planet. Sci. Lett.* 240, 529–536.
819 <http://dx.doi.org/10.1016/j.epsl.2005.09.030>.

820 Lin, J. F., Speziale, S., Mao, Z., Marquardt, H., 2013. Effects of the Electronic Spin Transitions of
821 Iron in Lower Mantle Minerals: Implications for Deep Mantle Geophysics and Geochemistry.
822 *Rev. Geophys.* 51, 244-275.

823 Lin, J. F., Wenk, H. R., Voltolini, M., Speziale, S., Shu, J., Duffy, T. S., 2009. Deformation of
824 lower-mantle ferropervicite (Mg,Fe)O across the electronic spin transition. *Phys. Chem.*
825 *Miner.* 36, 585–592.

826 Lin, J.F., Vankò, G., Jacobsen, S.D., Iota, V., Struzhkin, V.V., Prakapenka, V. B., Kuznetsov, A.,
827 Yoo, C.S. (2007) Spin transition zone in Earth's lower mantle. *Science*, 317, 1740-1743.

828 Lin, J.F., Heinz, D.L., Mao, H., Hemley, R.J., Devine, J.M., Li, J. and Shen, G. 2003. Stability of
829 magnesiowüstite in Earth's lower mantle. *PNAS*, 100, 4405-4408.

830 Lyubetskaya T., Korenaga J., 2007. Chemical composition of Earth's primitive mantle and its
831 variance: 1. method and results. *J. Geophys. Res.* 112, B03211. doi:10.1029/2005JB004223

832 Lyubutin, S., Gavriiliuk, A. G., Frolov, K. V., Lin, J. F., Troyan, I. A., 2009. High_Spin–Low_Spin
833 Transition in Magnesiowüstite ($Mg_{0.75}Fe_{0.25}O$) at High Pressures under Hydrostatic
834 Conditions. *J. of Experim. Theoret. Phys. Lett.*, 90, 617–622

835 Madi, K., Forest, S., Cordier, P., Boussuge, M. (2005) Numerical study of creep in two-phase
836 aggregates with a large rheology contrast: implications for the lower mantle. *Earth Planet. Sci.*
837 *Lett.*, 237, 223-238.

838 Mainprice, D., 2007. Seismic anisotropy of the deep Earth from a mineral and rock physics
839 perspective, *Treatise Geophys.*, 2, 437–491

840 Mao, W.L., Mao, H.K., Sturhahn, W., Zhao, J.Y., Prakapenka, V.B., Meng, Y., Shu, J.F., Fei,
841 Y.W., Hemley, R.J., 2006. Iron-rich post-perovskite and the origin of ultralow-velocity zones.
842 *Science*, 312, 564–565.

843 Matas J., Bass J., Ricard Y., Mattern E. and. Bukowinski M. S. T. , 2007. On the bulk composition
844 of the lower mantle: predictions and limitations from generalized inversion of radial seismic
845 profiles. *Geophys. J. Int.* 170, 764–780.

846 Mattern, E., Matas, J., Ricard, Y., Bass J.D., 2005. Lower mantle composition and temperature
847 from mineral physics and thermodynamic modelling, *Geophys. J. Int.*, 160, 973–990.

848 McDonough W.F., Sun S., 1995. The composition of the Earth. *Chem. Geol.* 120, 223–
849 253.[doi:10.1016/0009-2541\(94\)00140-4](https://doi.org/10.1016/0009-2541(94)00140-4).

850 McNamara, A.K., Garnero, E.J., Rost, S., 2010. Tracking deep mantle reservoirs with ultra-low
851 velocity zones. *Earth Planet. Sci. Lett.* 299, 1–9.[http://dx. doi.: 10.1016/j.epsl.2010.07.042](http://dx.doi.org/10.1016/j.epsl.2010.07.042).

852 Merli, M., Sciascia, L., Pavese, A., Diella, V., 2015. Modelling of thermo-chemical properties over
853 the subsolidus MgO–FeO binary, as a function of iron spin configuration, composition and
854 temperature. *Phys. Chem. Min.* 42, 347-362.

855 Merli, M., Bonadiman, C., Diella, V., Pavese, A. 2016. Lower mantle hydrogen partitioning
856 between periclase and perovskite: A quantum chemical modelling. *Geoch., Cosmochim. Acta*
857 173, 304-318.

858 Miyajima, Y., Ueda, T., Adachi, H., Fujii, T., Onaka, S., Kato, M. (2014) Dislocation density of
859 FCC metals processed by ARB. 6th International Conference on nanomaterials by severe plastic
860 deformation. IOP Conf. Series: materials Science and Engineering, 63, 012138,
861 doi:10.1088/1757-899X/63/1/012138.

862 Miyajima, N., Yagi, T., Hirose, K., Kondo, T., Kiyoshi Fujino, K., Miura, H. 2001. Potential host
863 phase of aluminum and potassium in the Earth's lower mantle. Am. Mineral., 86, 740-746.

864 Muir, J., Brodholt, J. 2015. Elastic properties of ferropericlase at lower mantle conditions and its
865 relevance to ULVZs. Earth Planet. Sci. Lett., 417, 40-48.

866 Murakami, M., Hirose, K., Sata, N., Ohishi, Y., 2005. Post - perovskite phase transition and
867 mineral chemistry in the pyrolitic lowermost mantle. Geophys. Res. Lett., 32, L03304,
868 doi:10.1029/2004GL021956.

869 Murakami, M., Ohishi, Y., Hirao, N., Hirose, K., 2012. A perovskitic lower mantle inferred from
870 high-pressure, high-temperature sound velocity data. Nature 485, 90–94.
871 <http://dx.doi.org/10.1038/nature11004>.

872 Nakajima, Y, Frost D.J., Rubie, D.C., 2012. Ferrous iron partitioning between magnesium silicate
873 perovskite and ferropericlase and the composition of perovskite in the Earth's lower mantle. J
874 Geophys. Res. 117:B08201.

875 Narygina, O., Dubrovinsky, L., Samuel, H., McCammon, C., Kantor, I., Glazyrin, I., Pascarelli, S.,
876 Aquilanti, G., Prakapenka, V., 2011. Chemically homogeneous spin transition zone in Earth's
877 lower mantle. Phys. Earth Planet. Inter. 185, 107–111.

878 Nomura, R., Ozawa, H., Tateno, S., Hirose, K., Hernlund, J., Muto, S., Ishii, H., Hiraoka, N., 2011.
879 Spin crossover and iron-rich silicate melt in the Earth's deep mantle. Nature473, 199–202.

880 Oganov, A., Dorogokupets, P.I., 2003. All-electrons and pseudopotential study of MgO: equation of
881 state, anharmonicity and stability. Phys. Rev. B 67, 224110-1/11.

882 Ono, S., 2008. Experimental constraints on the temperature profile in the lower mantle. *Phys.*
883 *Earth Planet. Inter.*, 170, 267–273, doi:10.1016/j.pepi.2008.06.033.

884 Ono, S., and A. R. Oganov (2005), In situ observations of phase transition between perovskite and
885 CaIrO_3 -type phase in MgSiO_3 and pyrolitic mantle composition, *Earth Planet. Sci. Lett.*, 236,
886 914-932.

887 Ohta, K., Fujino, K., Y. Kuwayama, Y., Kondo, T., Shimizu, K. and Ohishi Y. (2014) Highly
888 conductive iron-rich $(\text{Mg,Fe})\text{O}$ magnesiowüstite and its stability in the Earth's lower mantle, *J.*
889 *Geophys. Res. Solid Earth*, 119, 4656–4665, doi:10.1002/2014JB010972.

890 Otsuka, K., McCammon, C.A., Karato, S. (2010) Tetrahedral occupancy of ferric iron in $(\text{Mg,Fe})\text{O}$:
891 Implications for point defects in the Earth's lower mantle. *Phys. Earth Plan. Int.*, 180, 179-188.

892 Ottonello, G., Civalleri, B., Ganguly, J., Perger, W.F., Belmonte, D., Vetuschi Zuccolini, M., 2010.
893 Thermo-chemical and thermo-physical properties of the high pressure phase Anhydrous B
894 $(\text{Mg}_{14}\text{Si}_5\text{O}_{24})$: an ab initio all-electron investigation. *Am. Mineral.* 95, 563–573.

895 Ottonello G. (1997) *Principles of Geochemistry*, Columbia University Press, New York, 897 pp.

896 Pamato, M.G, Kurnosov, A., Boffa Ballaran, T., Trots, D.M., Caracas, R. Frost, D.J. 2014.
897 Chemistry and Mineralogy of Earth's Mantle. Hexagonal
898 $\text{Na}_{0.41}[\text{Na}_{0.125}\text{Mg}_{0.79}\text{Al}_{0.085}]_2[\text{Al}_{0.79}\text{Si}_{0.21}]_6\text{O}_{12}$ (NAL phase): Crystal structure
899 refinement and elasticity. *Am. Mineral.*, 99, 1562-1569.

900 Paktunc, A.D., 1998. MODAN: An interactive computer program for estimating mineral quantities
901 based on bulk composition. *Comput. Geosci.-UK*, 22(5), 425-431.

902 Prescher, C., Langenhorst, F., Dubrovinsky, L., Prakapenka, V., Miyajima, N., 2014. The effect of
903 Fe spin crossovers on its partitioning behavior and oxidation state in a pyrolitic Earth's lower
904 mantle system. *Earth Planet. Sci. Lett.* 399, 86–91.

905 Reali, R., Boioli, F., Gouriet, K., Carrez, P., Devincre, B., Cordier, P. (2017) Modelling plasticity of
906 MgO by 2.5D dislocation dynamics simulations. *Mat. Sciences and Engin.*, 690, 52-61.

907 Richet, P., Mao, H.-K., Bell, P. M., 1989. Bulk moduli of magnesiowüstites from static
908 compression experiments. *J. Geoph. Res.*, 94, 3037–3045.

909 Rost, S., Garnero, E.J., Williams, Q., Manga, M., 2005. Seismological constraints on a possible
910 plume root at the core–mantle boundary. *Nature* 435 (7042), 666–669.

911 Sakai, T., Ohtani, E., Terasaki, H., Sawada, N., Kobayashi, Y., Miyahara, M., Nishijima, M., Hirao,
912 N., Ohishi, Y., Kikegawa, T., 2009, Fe–Mg partitioning between perovskite and ferropericlaese
913 in the lower mantle. *Am. Mineral.*, 94, 921–925.

914 Sanchez, J. M., Ducastelle, F. Gratiias, D. 1984. Generalized cluster description of multicomponent
915 systems. *Phys. A.* 128, 334-350.

916 Scanavino, I., Prencipe, M., 2013, Ab-initio determination of high-pressure and high-temperature
917 thermoelastic and thermodynamic properties of low-spin (Mg_{1-x}Fe_x)O ferropericlaese with x in the
918 range [0.06, 0.59]. *American Mineralogist*, Volume 98, 1270–1278.

919 Scanavino, I., Belousov, R., Prencipe M., 2012. Ab initio quantum-mechanical study of the effects
920 of the inclusion of iron on thermoelastic and thermodynamic properties of periclaese (MgO).
921 *Phys. Chem. Miner.*, 39, 649–663.

922 Sidorin, I., Gurnis, M., Helmberger, D. V., 1999. Evidence for a ubiquitous seismic discontinuity at
923 the base of the mantle. *Science*, 286, 1326–1331, doi:10.1126/science.286.5443.1326.

924 Sinmyo, R., Hirose, K., 2013. Iron partitioning in pyrolitic lower mantle. *Phys. Chem. Miner.* 40,
925 107–113.

926 Sinmyo, R., Hirose, K., Nishio-Hamane, D., Seto, Y., Fujino, K., Sata, N., Ohishi, Y., 2008.
927 Partitioning of iron between perovskite/postperovskite and ferropericlaese in the lower mantle. *J.*
928 *Geoph. Res.*, 113, B11204, doi:10.1029/2008JB005730

929 Stølen S., Grande, T., 2004. *Chemical Thermodynamics of Materials: Macroscopic and*
930 *Microscopic Aspects.* John Wiley and Sons Ltd.

931 Stixrude, L., Lithgow-Bertelloni, C., 2007. Influence of phase transformations on lateral
932 heterogeneity and dynamics in Earth's mantle. *Earth Planet. Sci. Lett.* 263, 45–55.

933 Thorne, M.S., Garnero, E.J., Jahnke, G., Igel, H., McNamara, A.K., 2013. Mega ultra-low velocity
934 zone and mantle flow. *Earth Planet. Sci. Lett.* 364, 59–67.
935 <http://dx.doi.org/10.1016/j.epsl.2012.12.034>.

936 Tommaseo, C.E., Devive, J., Merkel, S., Speziale, S., Wenk, H.R. (2006) Texture development and
937 elastic stresses in magnesiowüstite at high pressure. *Phys. Chem. Min.*, 33, 84-97.

938 Trampert, J., Deschamps, F., Resovsky, J. S., Yuen, D. A. , 2004. Probabilistic tomography maps
939 chemical heterogeneities throughout the lower mantle. *Science*, 306, 853–856,
940 doi:10.1126/science.1101996.

941 Tsuchiya, T., Wentzcovitch, R.M., da Silva, C.R.S., de Gironcoli, S., 2006. Spin transition in
942 magnesiowüstite in Earth's lower mantle. *Phys. Rev. Lett.*, 96, 198501.

943 Valerio, G. , Catti, M., Dovesi, R., Orlando, R., 1995. Ab initio study of antiferromagnetic rutile-
944 type FeF₂. *Phys. Rev. B*, 52, 2422-2427.

945 van Orman, J.A., Fei, Y., Hauri, E.H., Wang, J. (2003) Diffusion in MgO at high pressures:
946 constraints on deformation mechanisms and chemical transport at the core-mantle boundary. *J.*
947 *Geophys. Res.*, 30, 1056.

948 van Westrenen, W., Li, J., Fei, J., Frank, M.R., Hellwig, H., Komabayashi, T., Mibef, K.,
949 Minarik, W.G., Van Orman, J.A., Watson, H.C., Funakoshi, K., Schmidt. M.W., 2005.
950 Thermoelastic properties of (Mg_{0.64}Fe_{0.36})O ferropericlae based on in situ X-ray diffraction to
951 26.7 GPa and 2173 K. *Phys. Earth Planet. Int.*, 151, 163–176

952 Vassiliou, M. S., Ahrens, T. J., 1982. The equation of state of Mg_{0.6}Fe_{0.4}O to 200 GPa. *Geoph.*
953 *Res.Lett.*, 9, 127–130.

954 Vilella K., Shim S-H., Farnetani C.G., Badro, J. 2015. Spin state transition and partitioning of iron:
955 Effects on mantle dynamics. *Earth and Planet. Sci. Lett.*, 417, 57-66.

956 Wang, X., Tsuchya, T., Hase, A. (2015) Computational support for a pyrolytic lower mantle
957 containing ferric iron. *Nature geoscience Letters*, 8, 556-560.

958 **Wdowik, U.D., Piekarz, P., Jochym, P.T., Parlinski, K., Olés, A.M. (2015) Influence of isolated and**
959 **clustered defects on electronic and dielectric properties of wüstite. Phys. Rev. B, 91, 195111-**
960 **1/10.**

961 Wentzcovitch, R. M., Karki, B. B., Cococcioni, M. , de Gironcoli, S., 2004. Thermoelastic
962 properties of MgSiO₃-perovskite: insights on the nature of the Earth's lower mantle.
963 Phys.Rev. Lett. 92, 018501

964 Wentzcovitch, R. M., Justo, J.F., Wu, Z., da Silva, C.R.S., Yuen, D., Kohlstedt, D., 2009.
965 Anomalous compressibility of ferropericlase throughout the iron spin cross-over. Proc. the Nat.
966 Acad. Sci.106, 8447–8452.

967 Wicks, J.K., Jackson, A., Sturhahn, W., 2010. Very low sound velocities in iron-rich (Mg,Fe)O:
968 implications for the core–mantle boundary region. Geophys. Res. Lett.37, L153041 (5 pp).

969 Yuge, K., 2010. Cluster expansion approach for transmutative lattice systems. J. Phys Cond.
970 Matter, **22**, 125402 (9pp).

971 **Zha, C.S., Mao, H., Hemley, R.J. (2000) Elasticity of MgO and a primary pressure scale up to 55**
972 **GPa. PNAS, 97, 13494-13499.**

973 Zhang, J., Kostak, P., 2002. Thermal equation of state of magnesiowüstite (Mg_{0.6}Fe_{0.4})O. Phys.
974 Earth Planet. Inter., 129, 301– 311

975 Zhang, S., Cottaar, S., Liu, T., Stackhouse, S., Militzer, B., 2016. High-pressure, temperature
976 elasticity of Fe- and Al-bearing MgSiO₃: Implications for the Earth's lower mantle. Earth
977 Planet. Sci. Lett. 343, 264-273.

978

979 **CAPTIONS TO THE FIGURES**

980

981 **Figure 1.** Geotherms used in the present work, for LM and LLM. LM-geotherm with a potential
982 temperature of 1920 K at 24 GPa and a T -gradient (dT/dz) in the range of ~ 0.5 K/Km, is applied to
983 the mantle region of ~ 24 -80 GPa (solid blue line). LLM-geotherm, with a potential temperature of
984 2615 K at 96 GPa and dT/dz of ~ 0.85 K/Km, is considered in the mantle region of ~ 80 -130 GPa
985 (solid red line). The consolute temperature curves, T_C calculated for LS (solid black line) and HS
986 (dashed black line) state of iron as a function of P are also shown. Miscibility gap ($T_C > T_{\text{geotherm}}$)
987 occurs between 23 and 42 GPa for LS only.

988

989 **Figure 2.** Predicted miscibility gap for LS in the MgO–FeO binary system, as a function of pressure
990 and temperature. P - T values from the geotherms here used. The pyrolitic Fe-periclase reference x_0 -
991 composition ($x=0.175$ FeO) is also reported.

992

993 **Figure 3.** LS: blue; HS: red. (a) Compositions of the x_0 -, x_1 - and x_2 -phases (solid, dashed and
994 dotted lines, respectively) in terms of FeO fractions; (b) phase proportions λ_0 , λ_1 and λ_2 (solid,
995 dashed and dotted lines, respectively) of x_0 -, x_1 - and x_2 -mixings, respectively.

996

997 **Figure 4.** LS: blue; HS: red. (a) The average equilibrium constant, $\langle K(P,T) \rangle$, is plotted according
998 to eq.(7-11) in the text, along the LM-LLM-paths; (b) static excess enthalpy (ΔH_{excess}) determined
999 at 24/1900-107/2910 GPa/K, as an example of the LM and LLM mantle regions, respectively.

1000

1001 **Figure 5.** Density (g cm^{-3}) of the x_0 -, x_1 - and x_2 -phases (solid, dashed and dotted lines,
1002 respectively) in the case of LS (blue) and HS (red).

1003

1004 **Figure 6.** LS: blue; HS: red. FeO-fraction excess with respect to the reference x_0 -composition due
1005 to exchange between Fe-periclase and *reservoir*, in open (Mg,Fe)O-system.